June 2002 • NREL/SR-590-31983

Subcontractor Report

Characterization of and Ti Gettering for PV Substrates

Final Subcontract Report
28 January 1998 – 28 August 2001

G.A. Rozgonyi, A. Karoui, A. Romanowski, and L. Kordas
North Carolina State University
Raleigh, North Carolina

National Renewable Energy Laboratory

1617 Cole Boulevard
Golden, Colorado 80401-3393

NREL is a U.S. Department of Energy Laboratory
Operated by Midwest Research Institute • Battelle • Bechtel

Contract No. DE-AC36-99-GO10337

June 2002 • NREL/SR-590-31983

Characterization of and Ti Gettering for PV Substrates

Final Subcontract Report
28 January 1998 – 28 August 2001

G.A. Rozgonyi, A. Karoui, A. Romanowski, and L. Kordas
North Carolina State University
Raleigh, North Carolina

NREL Technical Monitor: R. McConnell

Prepared under Subcontract No. XAF-8-17607-03

National Renewable Energy Laboratory

1617 Cole Boulevard
Golden, Colorado 80401-3393

NREL is a U.S. Department of Energy Laboratory
Operated by Midwest Research Institute • Battelle • Bechtel

Contract No. DE-AC36-99-GO10337

NOTICE

Available electronically at http://www.osti.gov/bridge

Available for a processing fee to U.S. Department of Energy
and its contractors, in paper, from:

U.S. Department of Energy
Office of Scientific and Technical Information
P.O. Box 62
Oak Ridge, TN 37831-0062
phone: 865.576.8401
fax: 865.576.5728
email: reports@adonis.osti.gov

Available for sale to the public, in paper, from:

U.S. Department of Commerce
National Technical Information Service
5285 Port Royal Road
Springfield, VA 22161
phone: 800.553.6847
fax: 703.605.6900
email: orders@ntis.fedworld.gov
online ordering: http://www.ntis.gov/ordering.htm

Printed on paper containing at least 50% wastepaper, including 20% postconsumer waste

TABLE OF CONTENTS

Project Overview

The initial project objectives were twofold; namely, to determine the optical and gettering properties of titanium and titanium oxy-nitride films, and to examine the influence of carrier recombination processes on the microwave reflection coefficient in the frequency domain such that PV materials parameters could be evaluated non-destructively. A third topic was added as the main focus of our six month contract extension, wherein we carried out a detailed characterization study of dislocated, high purity, float zone crystals grown at NREL by Ted Cizsek. These were compared with nitrogen doped CZ wafers. The accompanying report has a chapter devoted to each of these topics presented in reverse order of the above list. Highlights of these chapters include the following

.

With regard to dislocated FZ material we note that the average carrier lifetimes of 50 to 100 microseconds in heavily dislocated areas are still quite high for PV applications. This is attributed to the fact that the dislocations are "clean" in this high purity FZ crystal and relatively inactive electrically. This relatively low impact of a high density of dislocations on minority carrier recombination lifetime leads us to believe that the proper tailoring of SiO_2 precipitation phenomena will enable long diffusion length PV wafers to be produced which also exhibit enhanced mechanical yield behavior. Thus, the above ongoing electrical/structural approach is being extended to low oxygen content CZ wafers, as well as FZ wafers with deliberately added concentrations of oxygen. In addition, a processing bonus related to a near surface defect band induced surface texture in nitrogen doped CZ wafers is likely to have a positive impact on single crystal PV devices by simultaneously providing surface texturing and a near surface gettering sink for bulk impurities.

The microwave photoconductance method was a relation for the microwave reflection coefficient in the frequency domain was found. A single level Shockley-Read-Hall non-stationary recombination model was used for the description of the carrier kinetics. Although six parameters, i.e., surface recombination velocity v_s, diffusivity D_n, activation energy E_r, electron/hole capture cross sections σ_n, σ_p, and concentration N_r were analyzed, only four are robust; namely v_s, E_r, $N_r c_n$ and σ_p/σ_n, and among them two, E_r and σ_p/σ_n, can be used as material parameters. These two parameters were evaluated from the frequency resolved spectra for silicon wafers intentionally contaminated with Ni and Fe. The E_r and σ_p/σ_n values obtained for Fe, and Fe+Ni contaminated wafers were equivalent, while in the presence of Ni, the above parameters were different, indicating that these parameters can be used for material characterization

The titanium thin film study revealed that a TiN_xO_y film exhibits the best optical quality; however, poor interface formation between the film and surface due to strong Ti and O bonds eliminates that film as a good external getter. Both Ti and TiN_x films have good gettering properties, however they have poor optical parameters. The long wavelength reflectance for both these films is high and reaches a value between 40 to 50%. A short wavelength reflectance of 20% for a Ti film is lower than the reflectance for TiN_x and is probably caused by surface roughness, which is the largest for Ti film. Following thermal gettering treatments, semiconducting films are formed with an optical bandgap between 1.6eV and 2.8eV.

Chapter 1

Characterization of Controlled Defect/Impurity Growth of Float Zone Crystals

INTRODUCTION

Although many aspects of the optimization of silicon crystal growth and wafer processing for producing integrated circuit (IC) devices enable improvements in crystalline photovoltaic(PV) processing, a major defect engineering difference between IC and PV substrates is related to the dominant impurity oxygen. On the one hand, low oxygen wafers from float zone(FZ) grown ingots are the purest materials with the highest minority carrier lifetime [i]. These wafers generally produce the highest efficiency planar and concentrator solar cells. However, FZ material suffers the highest yield losses due to breakage and mechanical failure, as well as performance degradation due to slip dislocations. On the other hand, controlled internal silicon dioxide precipitation gettering of high oxygen Czochralski(CZ) wafers with a tailored near-surface denuded zone, which has become the primary starting material for the IC community, also provides wafers with the best mechanical strength for the unique requirements of PV processing, e.g., texturing. Unfortunately, the CZ wafers suffer from minority carrier lifetime degradation due to bulk recombination at the oxygen precipitates, particularly if they have been decorated by metallic impurities. Thus, since breakage and yield/performance improvements are key issues for the thinner PV CZ wafers, it is important to examine the basic mechanisms and interplay between oxygen hardening, oxygen precipitation lifetime degradation, the impact of nitrogen doping, and the crystal response to the presence of metallic impurities.

The research program at NCSU has been initiated on ultra high purity CZ and FZ silicon wafers supplied by NREL and the member companies of SiWEDS, an NSF sponsored Industry/University consortium of silicon vendors and integrated circuit processing companies. This resource base has been supplemented by representative material from the PV community, and is directed towards an in-depth examination of those mechanical yield and bulk lifetime issues mentioned above. In addition, we are examining the temperature dependent electrical activity of dislocations in high lifetime, ultrapure silicon to determine the underlying energy levels associated with undecorated individual dislocations. The intent is to use these wafers to extend the study to metal impurity contaminated individual and bunched dislocation/grain boundary environments. A final and extremely important consideration is the dynamic state of point defects in those wafer regions which are dislocation free. Although extended defects and impurities in silicon are often specified to have a certain density or concentration, it is often the balance between lattice vacancies and interstitials and their mutual interaction/condensation into dislocations/voids which dictates the quality of a crystal/wafer during growth/processing.

HISTORY

Float zone crystals are known to be quite vulnerable to the generation and movement of dislocations, as illustrated in the x-ray topographic(XRT) images presented in the middle pair of scribed wafers in Fig. 1 (from the work of Abe, et al[ii]), following a single or double thermal cycle of 1150C. An FZ crystal strengthened by nitrogen doping to 4.5 E 14cm^{-3}, see the lower pair of XRT in Fig. 1, is dramatically improved to the point where the N doped FZ wafer is actually more resistant to dislocation formation than the CZ wafer, see upper pair of XRTs. It has been shown that nitrogen atoms and their related defect complexes are effective in enhancing the nucleation of oxynitride precipitates, which produce a dislocation locking action that is about 100 times more effective than that provided by homogeneous oxygen precipitation[iii]. In addition, for low oxygen CZ crystals, which do not produce adequate precipitation for IC internal gettering, nitrogen doping will initiate a gettering action at oxynitride aggregates. This is currently a very active area of study for IC wafer production[iv] for two reasons. First, since lower oxygen is achieved by reduced dissolution of quartz crucibles, this also translates into lower levels of metallic impurities. Secondly, nitrogen complexing with vacancies greatly reduces the size and density of octahedral void defects, which are a serious IC yield limiting crystal defect. This point is important in creating defect engineering options for PV applications, which will depend on balancing the vacancy/interstitial and nitrogen/oxygen concentrations such that the wafers are "hard" and charge carriers have a long lifetime.

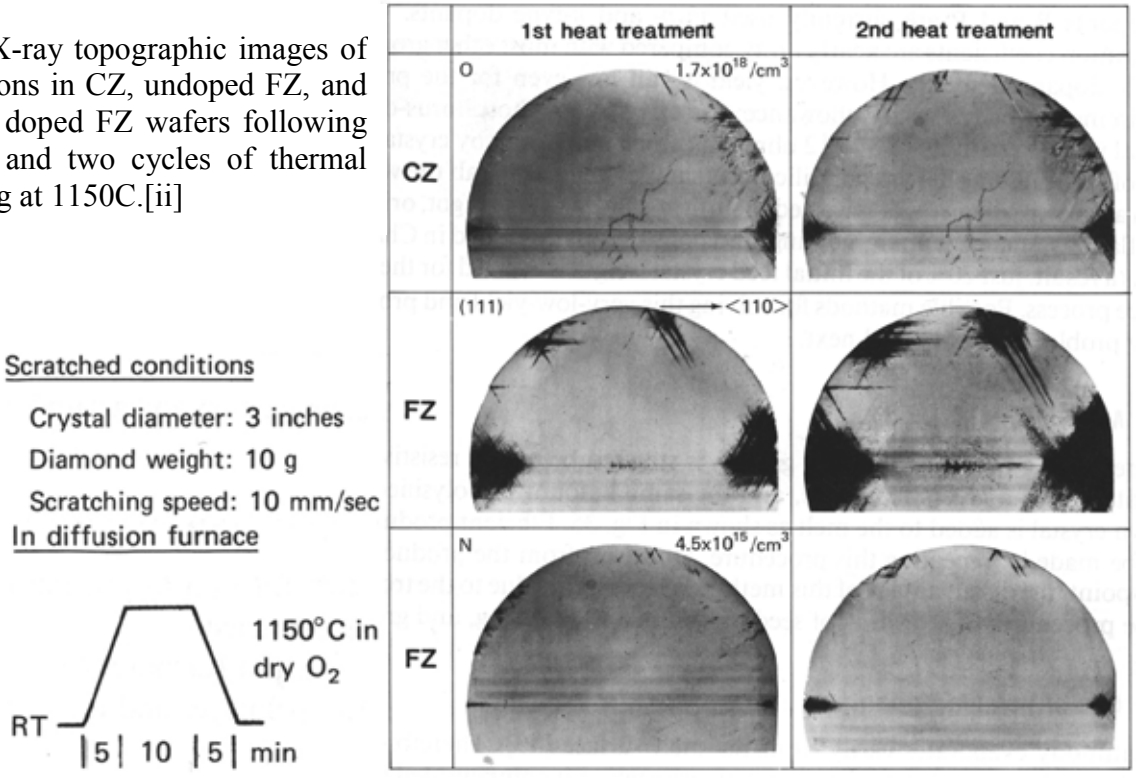

Fig. 1: X-ray topographic images of dislocations in CZ, undoped FZ, and nitrogen doped FZ wafers following scribing and two cycles of thermal annealing at 1150C.[ii]

RECENT ACTIVITY

Next, we present new results on electrical(recombination lifetime) and structural(dislocation density) correlations in high purity, undoped FZ crystals which serve to illustrate the diagnostic tools available and the approach underway at NCSU. Fig. 2 compares the same axial wafer from an NREL ingot examined at NCSU in a non-destructive fashion by both x-ray topography, see Fig. 2(a), and laser-microwave photoconductance decay, see Fig. 2(b). As expected, the highest lifetimes correspond to the low dislocation density areas; however, it is important to note that the average values of 50 to 100 microseconds in the heavily dislocated areas are still quite high, particularly for PV applications. This is attributed to the fact that the dislocations are "clean" in this high purity FZ crystal and relatively inactive electrically. Work is in progress to track the impact of gettering by adding controlled amounts of metallic impurities, and performing low temperature EBIC imaging and DLTS in addition to the lifetime mapping, to examine the electrical activity of specific defects and defect free regions. It is important to note that the relatively low impact of a high density of dislocations on minority carrier recombination lifetime shown in Fig. 2, leads us to believe that the proper tailoring of SiO_2 precipitation phenomena will enable long diffusion length PV wafers to be produced which also exhibit enhanced mechanical yield behavior. Thus, the above ongoing electrical/structural approach is being extended to low oxygen content CZ wafers, as well as FZ wafers with deliberately added concentrations of oxygen. The primary thrust will be the influence of nitrogen on the nucleation of oxygen precipitates via the formation of N-V complexes. The interaction of nitrogen with vacancies and interstitials will greatly impact the size and density of precipitates, as well as the

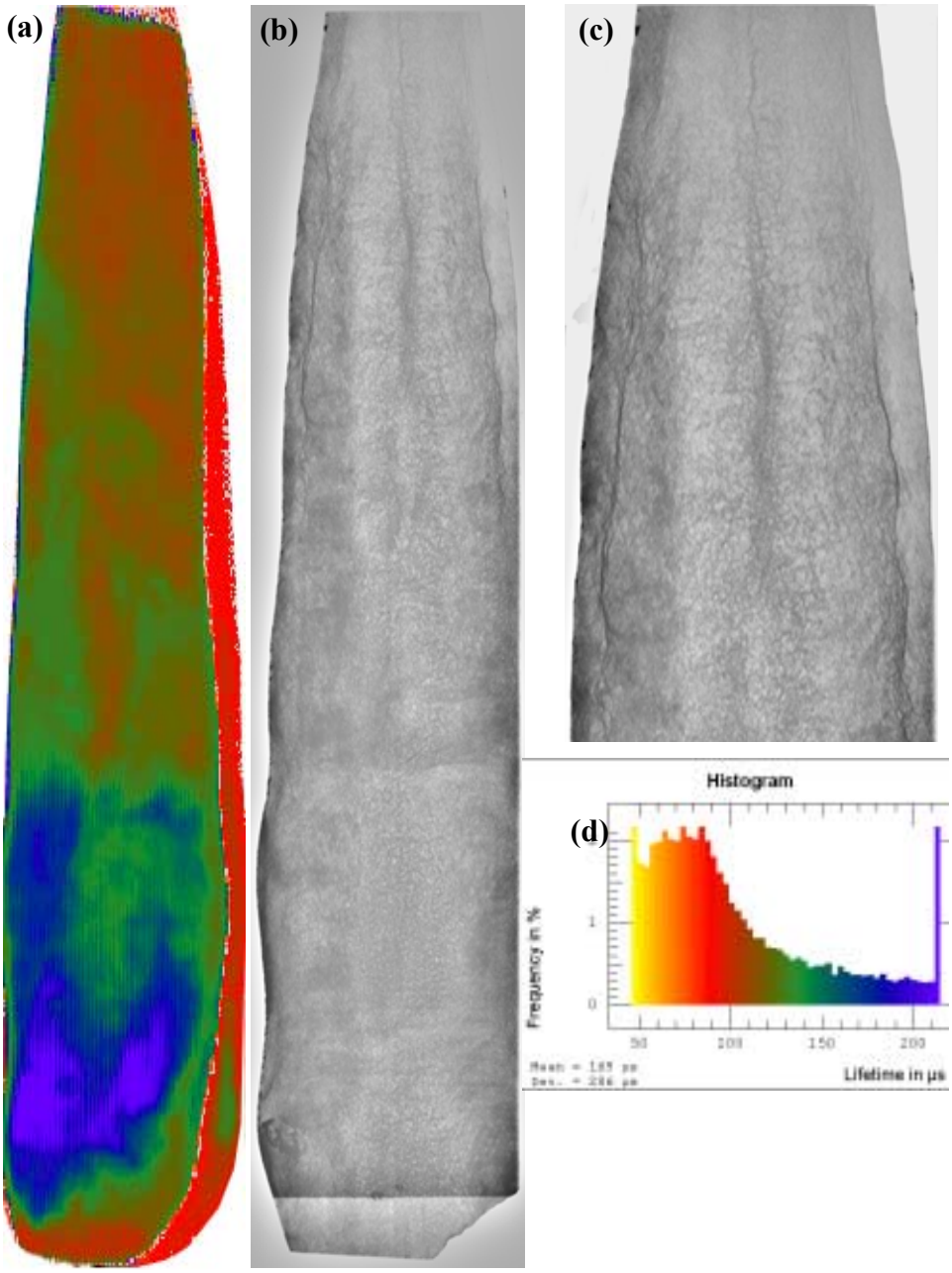

Fig. 2: Correlation between PCD lifetime map(a) and x-ray topographic image(b) for which specific defect regions are evident in both the axial and radial directions. The PCD determined minority carrier recombination lifetime distributions are tabulated in the color-coded histogram in the lower right(d). Note that as the crystal diameter is increased the resulting change in growth conditions produces a dramatic decrease in the dislocation density and increase in the lifetime. In addition, the enlarged XRT image at the upper right(c) indicates strong radial changes in dislocation density occur. The presence of defect "lineage" is also evident just inside the ingot edge and at its center. The corresponding lifetime variations are evident in frame(a).

nucleation and motion of dislocations. The intent is to vary the oxygen content as a means to merge and examine the primary difference between FZ and CZ crystals, and the nitrogen content to increase the hardness of both systems while reducing the recombination at precipitates.

PROCESSING "BONUS" DUE TO UNANTICIPATED SURFACE TEXTURE RESULTS

Next we describe recent results on N-CZ wafers that are likely to have a positive impact on single crystal PV devices by simultaneously providing surface texturing and a near surface gettering sink for bulk impurities. An unusual defect band has been found [v] within the outer micron of the traditional defect free denuded zone in N-CZ wafers, as revealed in Fig. 3(a) by the defect density depth profile obtained by Oxygen Precipitate Profiler (OPP). The SIMS O and N

profiles in Fig. 3(b) show a clear correlation of the O and N distributions in that thin surface defect band. Although Fig. 3(a) and (b) were done on materials grown in different conditions and the temperature of the nucleation step (Lo), had a 100 degrees difference, the defects appear to be due to an interaction between N and O atoms while diffusing and clustering in the vicinity of the wafer surface.

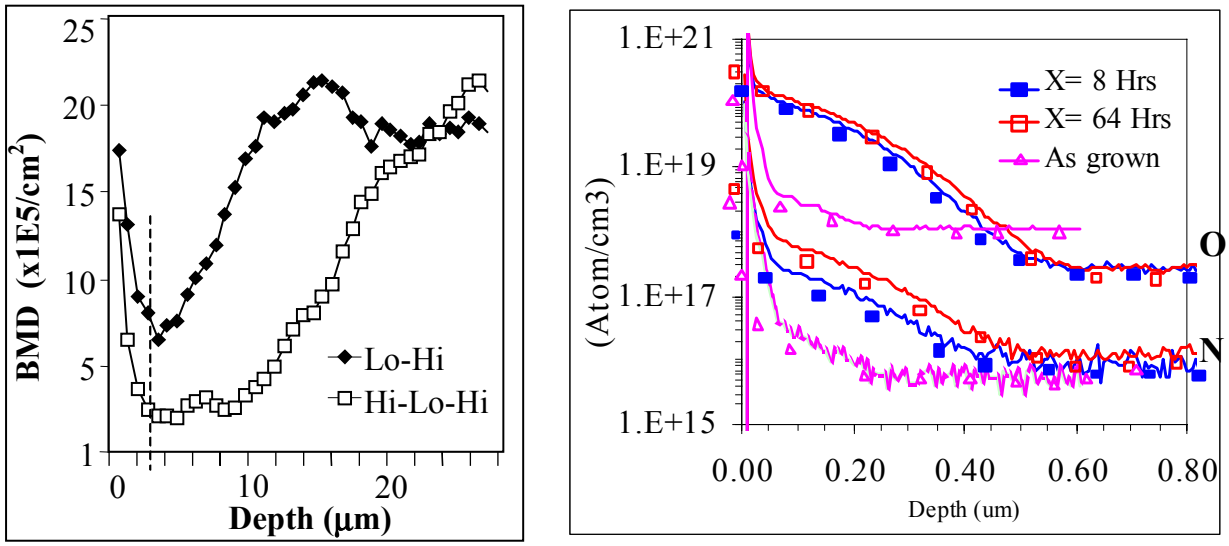

(a) (b)

Fig. 3: (a) OPP bulk micro defect distributions of Lo-Hi and Hi-Lo-Hi heat treated N-Cz Si samples (Hi at 1250C for 1 hr, Lo at 650C for 8 hrs, Hi at 1050C for 16 hrs).
(b) O and N SIMS profiles at the surface of an as grown and heat treated N-Cz Si samples by Lo-Hi process (750C/ X hr + 1050C/16hr).

TEM images in Fig. 4(a) and (b) show precipitates labeled (1) and (3). The unusual heavy and near surface localized oxide precipitation is accompanied by the formation of stacking faults labeled (4) and dislocations.

Upon annealing and etching, this near surface gettering band of defects fortuitously forms a very low reflectivity (<5%) textured surface, while the carrier diffusion length is increased due to the gettering. The defects are shown following preferential etching in Fig. 5(a) and Fig. 6, and in cross-section TEM in Fig. 4. The fact that it is nitrogen enhancing the nucleation of near-surface oxygen precipitation is evident from the SIMS depth profiles of N and O presented in Fig. 3(b). In connection to the above described surface defects, a manufacturing compatible process is currently being studied which would generate a surface micro-structure compatible with junction fabrication. This process consists of two simple etching steps (i) dense pit nucleation with the highly stress sensitive defect decoration of Wright etching, see Fig. 6(a), and followed by (ii) pit growth and gettering sink material removal using highly anisotropic etching in an alkali solution, see Fig. 6(b), which also removes any undesireable chemical traces from the Wright etching which might introduce junction contamination.

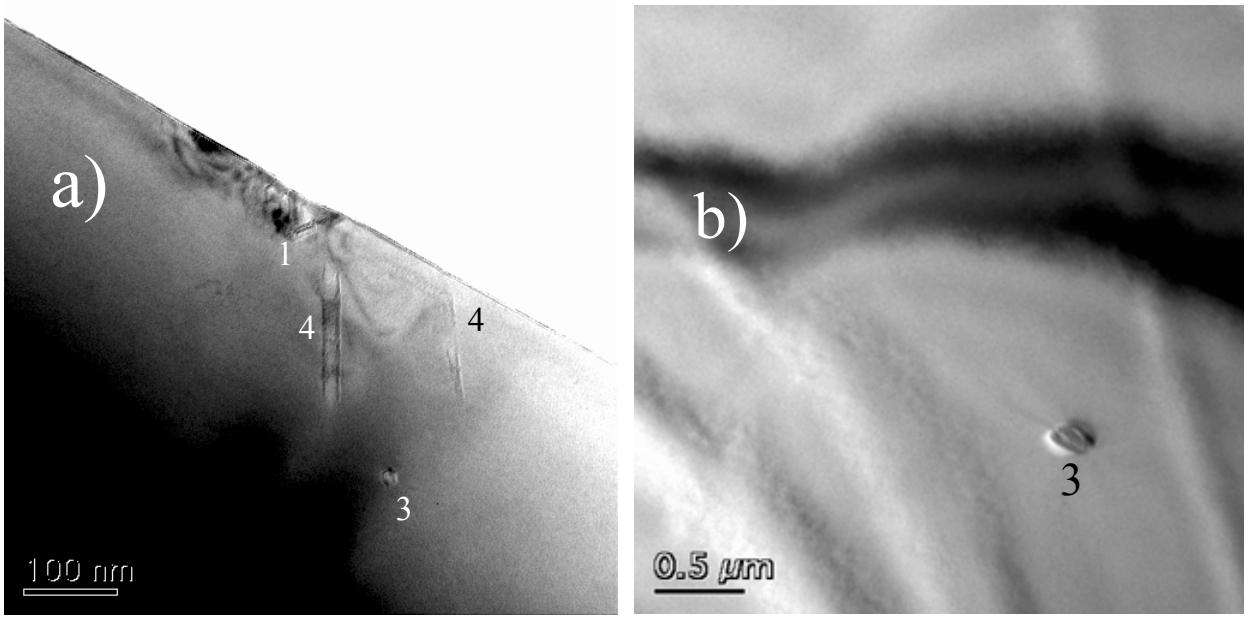

Fig. 4: HR TEM micrographs taken under two beam condition, illustrating the range of defects of an amorphous precipitate at the near surface (defect 1) and at a depth of 3µm (defect 3). Note the contrast change at the corner which reveals the stress variation due to the N.

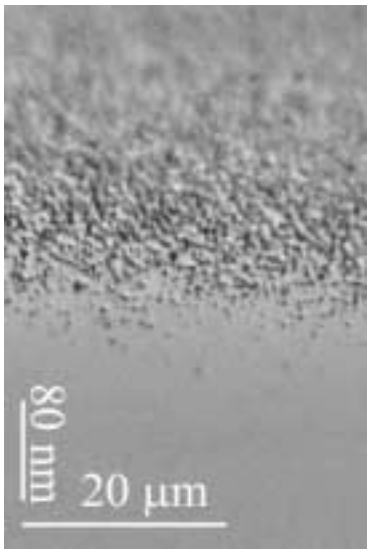

(a)

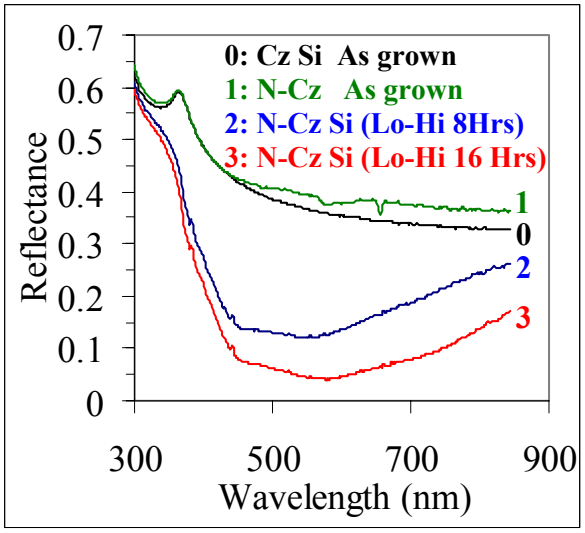

(b)

Fig. 5: a) Etch pits induced on a bevel polished N-CZ wafer surface by oxygen precipitation following a Lo-Hi anneal and 1 min of Wright etching,
b) Normal incidence specular reflectance of as-grown and annealed N-CZ Si, see curves 1-3, compared to conventional Si, curve 0, measured by a Filmetrics Model F20 Reflectometer with a detection solid angle of ~8°.

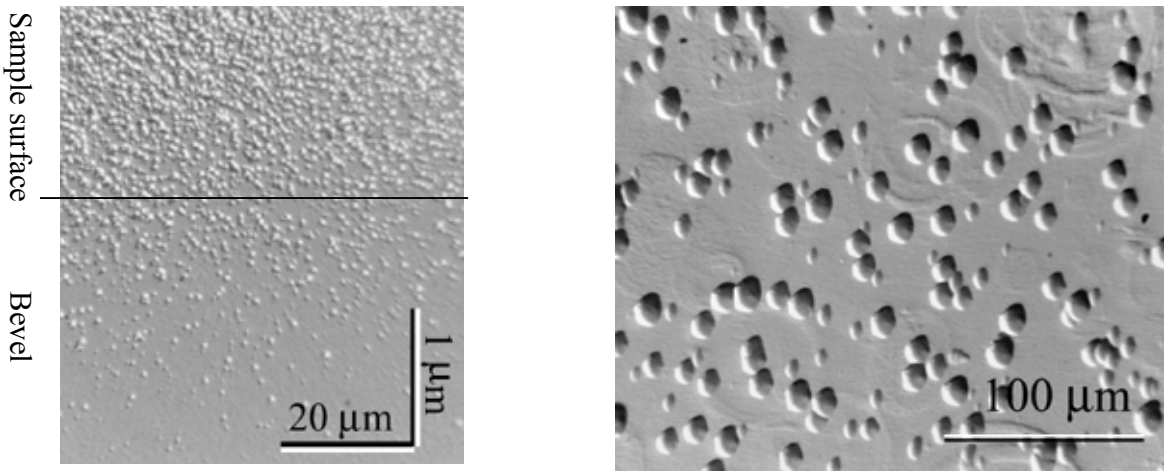

Fig. 6: Nomarski micrographs of N-CZ Si (111) beveled and Wright etched samples for 1 min (a) and a separate sample etched with KOH for 1 min (b).
High density of small etch pits are created by delineating the surface defects and pit grow and connect togethr with longer KOH etching time.

CONCLUSIONS

This report gives an update on the electrical behavior of dislocations in high purity float zone crystals, and the impact of nitrogen doping on the nucleation of oxygen precipitates. Our experimental results demonstrate that moderately high effective carrier lifetimes of 50 to 200 microseconds can be sustained in heavily dislocated FZ crystals. In N-CZ wafers PV defect engineering options are being explored based on new observations of near-surface defect nucleation and surface texturing. Enhanced light trapping, resulting in a specular reflectance below 5%, can be achieved while etching away surface gettering sinks introduced by the nitrogen doping.

REFERENCES

1. T.F.Ciszek, T.H.Wang, R.W.Burrows, T.Bekkedahl, M.I.Symko, J.D.Webb, Solar Energy Materials and Solar Cells **41/42**, 61 (1996).
2. T.Abe, K.Kikuchi, S.Shira, and S.Muraoka, in "Semiconductor Silicon/1981", H.R.Huff, J.Kriegler and Y.Takeishi, eds., p.54, Softbound Symp. Serv. Electrochem. Soc., Pennington, New Jersey, 1981.
3. K.Sumino, I.Yonenaga, M.Imai and T.Abe, J. Appl. Phys. **54**, 5016 (1983).
4. Nakai-K; Inoue-Y; Yokota-H; Ikari-A; Takahashi-J; Tachikawa-A; Kitahara-K; Ohta-Y; Ohashi-W J. App. Phys. **89**, 8; 4301, (2001).
5. Karoui et al, submitted to APL.

Chapter 2

Contactless Characterization of Silicon Wafers Using Frequency Resolved Photo Conductance Decay

INTRODUCTION

The contactless and non-destructive microwave photoconductance decay (μ-PCD) technique is routinely used to characterize carrier recombination lifetime in semiconductors. However, recombination center identification through determination of center concentration N_r, electron/hole capture cross-section σ_n, σ_p, and activation energy E_r remains an unresolved challenge. In principle, by using the Shockley-Read-Hall model, the values of these parameters can be determined by measuring the carrier lifetime transient characteristics [1,2,3,4,5,6,7]. Since each recombination center is characterized by a unique activity as a function of temperature or injection level, it should be possible to identify the center by applying nonlinear curve fitting procedures to these relationships. Nevertheless, in practice, the relatively small differences in their impact, together with the presence of interfering effects, such as surface recombination or multiple defect coexistence (each with different values of E_r, N_r, σ_n, σ_p), means that center identification using such methods remains difficult and often leads to questionable solutions. At present, it seems that there is no one general solution to this problem and novel alternative proposals need to be explored. The activation energy and the capture cross sections depend on temperature. Literature values for these parameters, although available for low[8] and high temperatures[9,10], are lacking for room and moderate temperatures.

Three dimensional analysis of the carrier transport generated by pulsed and sine modulated laser beam have been carried out by Otaredian[11,12] . He presented a theory based on diffusion carrier equations characterized by three parameters bulk carrier lifetime and two surface recombination velocities. Recently, Schieck[13] *et al* characterized silicon wafers by evaluation of the ambipolar diffusivity for different injection levels. In our study the recombination process is described by E_r, N_r, σ_n and σ_p, and their impact on the microwave reflection coefficient is investigated for different temperatures. The influence of surface recombination velocity on microwave reflection coefficient were analyzed in our previous works[14,15,16], where both in-phase and quadrature components of the microwave reflection coefficient were presented in a complex plane as Nyquist plots. It was shown that the Nyquist plot reduces to one arc for single level recombination process and two arcs in the case of trapping-recombination processes. In this paper, material parameters that can be uniquely evaluated from the reflectance spectra using a non-linear simplex fitting procedure 17 are investigated.

The paper is organized as follows. Firstly, a detailed analysis of the microwave reflection coefficient in the frequency domain is presented, which is based on the one-dimensional diffusion transport equation including minority carrier diffusion, surface recombination and carrier recombination at single recombination centers. Secondly, robust

parameters are selected which characterize the process. Finally, the material parameters are evaluated for p-type silicon containing Fe and Ni impurities, the results of which are compared with measured DLTS and μ-PCD data.

THEORY AND EVALUATION PROCEDURE

The AC component of the microwave reflection coefficient depends on the electron/hole mobilities μ_n, μ_p and electron/hole AC carrier concentrations[15] $\tilde{n}, \tilde{p}$:

$$\tilde{R}(\omega) = q\left(\frac{\partial R}{\partial \sigma}\right)_o \int_V (\mu_p \tilde{p} + \mu_n \tilde{n}) dV \tag{1}$$

where the volume V (or the microwave penetration depth for a one-dimensional case as considered here) is practically limited and is dependent on the microwave frequency and sample resistivity; it is estimated to be 500 μm for a 1 Ωcm resistivity sample using a frequency of 10 GHz.

The concentration of captured electrons n_r is described by the rate equation (2a) and depends on carrier transitions between the bands and the recombination centers[5]:

$$\frac{dn_r}{dt} = R_n - R_p \tag{2a}$$

$$R_n = c_n n(N_r - n_r) - c_n n_r n_1 \tag{2b}$$

$$R_p = c_p n_r n_1 - c_p (N_r - n_r) p_1 \tag{2c}$$

where R_n (R_p) describes the net rate of electron (hole) transitions from the conductance (valence) bands, while N_r is the recombination center concentration. The coefficients c_n, $(= v_T \sigma_n)$, c_p $(= v_T \sigma_p)$, are the electron, hole capture coefficients, respectively, and v_T is the thermal velocity. In the Shockley-Read-Hall (SRH) classical approach, a steady state case is analyzed with R_n equal to R_p. In this work, we assume (i) non-steady state condition at recombination center ($R_n \neq R_p$) and (ii) low excess carrier concentration. The second assumption allows linear equations to be used (2) by introduce the following relations[5,16]: $n = n_o + \delta n$ for electrons, holes, and captured electrons, respectively. Thus Eqs. (2) can be rewritten as follows:

$$\frac{d\delta n_r}{dt} \approx \left(\frac{1}{\tau_n} - \frac{1}{\tau_p}\right)\delta n - M\delta n_r \tag{3}$$

where τ_n and τ_p are electron, hole lifetimes[5]:

$$\tau_n^{-1} = c_n N_r (1 - f_r) \quad , \tau_p^{-1} = c_p N_r f_r \tag{4}$$

while f_r is the electron occupancy function:

$$f_r = \frac{c_n n_o + c_p p_1}{c_n (n_o + n_1) + c_p (p_o + p_1)} \tag{5}$$

and:

$$n_1 = N_c \exp\left(-\frac{E_c - E_r}{kT}\right), \quad p_1 = N_v \exp\left(-\frac{E_r - E_v}{kT}\right) \tag{6}$$

E_r is the recombination center activation energy, n_o, p_o are dark-equilibrium electron, hole concentrations. The coefficient M in Eq. (3) is defined as follows: $M = \beta + \gamma$, $\beta = c_n (n_o + n_1)$, $\gamma = c_p (p_o + p_1)$. In order to eliminate unknown free hole concentration in Eq. (2) it is assumed that excess electron concentration is equal to the excess hole concentration (small N_r concentration):

$$\delta n = \delta p \tag{7}$$

The above local neutral condition is valid because the microwave frequency of 10 GHz corresponds to the microwave time period of 100 ps, which is much longer than the sample dielectric relaxation time[18] $\tau_D \approx 1$ps, ($\tau_D = \rho\varepsilon_s$, ρ is sample resistivity of ~1Ωcm and $\varepsilon_s = \varepsilon_o\varepsilon_r$ with $\varepsilon_r = \sim 12$ for Si). In the frequency domain, captured electron concentration has the form[19,20]:

$$\delta n_r = \tilde{n}_r \exp(i\omega t) \tag{8}$$

In a similar way one can describe the electron and hole excess concentrations. Inserting (8) to (3) one can determine $\tilde{n}_r$:

$$\tilde{n}_r = \tilde{n} \frac{\tau_n^{-1} - \tau_p^{-1}}{i\omega + M} \tag{9}$$

Relation (9) indicates that captured electrons concentration $\tilde{n}_r$ is a complex number, due to free carrier trapping process at a recombination center with a delay time of M^{-1}.

The free electron diffusion equation can be written as[19,20]:

$$\frac{\partial n}{\partial t} = D_n \frac{\partial^2 n}{\partial x^2} + g_n - R_n \tag{10a}$$

with generation function of g_n, recombination rate of R_n, and electron diffusivity of D_n. In a frequency domain, equation (10a) has the form (see Appendix):

$$\frac{\partial^2 \tilde{n}}{\partial x^2} - \kappa^2 \tilde{n} = -\frac{\tilde{g}}{D_n} \tag{10b}$$

where κ is a complex number described by $\kappa = \sqrt{1 + i\omega\tau_n - \Lambda}$ and:

$$\Lambda = \tau_n \beta \frac{\tau_n^{-1} - \tau_p^{-1}}{i\omega + M} \tag{11}$$

while g_n and $\tilde{g}$ are related as follows: $g_n = g_o + \tilde{g}\exp(i\omega t)$, and the AC electron-hole pair generation function $\tilde{g}$ has the form[19]:

$$\tilde{g} = \tilde{G}_t \alpha \exp(-\alpha x)/A \tag{12}$$

where α is the absorption coefficient, A the microwave head surface (equal to electron-hole generation area) and $\tilde{G}_t$ the total electron-hole generation coefficient. In the analyzed case here, the diffusion length $L_n (= \sqrt{D_n \tau_n})$ is much less than the wafer thickness; therefore, only carrier recombination process on the wafer surface $x = 0$ is taken into consideration and the wafer is assumed to be infinitely thick. Thus the boundary conditions have the form[19,20]:

$$D_n \frac{\partial \tilde{n}}{\partial x} = v_s \tilde{n}(0), \text{ and } \tilde{n}(x >> 1) = 0 \tag{13}$$

where v_s is the surface recombination velocity. Using diffusion equation (10b) and the above boundary condition, the AC free electron concentration $\tilde{n}$ can be found. The total (volume integrated) electron excess number $\tilde{N}(\omega)$ is given by the relation[14,15,19]:

$$\tilde{N}(\omega) = A\int_0^\infty \tilde{n}\,dx = \frac{\tilde{G}_t \tau_n}{\kappa^2 (1 + \alpha^*/\kappa)}\left(1 + \frac{\alpha^*/\kappa}{1 + S/\kappa}\right) \tag{14}$$

where S is the normalized surface recombination velocity, $S = v_s L_n / D_n$, and $\alpha^* = \alpha L_n$. Taking into account relations (1), (7) and (14) the AC microwave reflection coefficient can be expressed as:

$$\tilde{R}(\omega) = q\left(\frac{\partial R}{\partial \sigma}\right)_o \mu_n \left(1 + \frac{\mu_p}{\mu_n}\right)\tilde{N}(\omega) \tag{15}$$

The reflection coefficient $\widetilde{R}(\omega)$ is a complex number. Its imaginary part, $Y(\omega) = \mathrm{Im}(\widetilde{R}(\omega))$, can be described by a single Lorentzian[16,21], peaked at the frequency f_0, and having a maximum value, Y_0. The Lorentzian function is plotted for four temperatures (24, 80, 180 and 240°C) in Fig. 1a. The imaginary and real components can be used for constructing the Nyquist plot in the complex plane, as shown in Fig. 1b. In general, both f_0 and Y_0 depend on temperature, electron and hole capture cross-sections σ_n and σ_p, concentration N_r, and the activation energy E_r. As shown in Fig. 2, the dependence of f_0 and Y_0 on E_r is weak (for the midgap levels) at low temperatures, meaning that these levels are most accurately determined at elevated temperatures. It is interesting to analyze a simple case with $\Lambda = 0$ where the carrier lifetime is described by one parameter τ ($= \tau_n = \tau_p$). From relations (4) one can show that relation $\Lambda = 0$ holds for $f_r = \left(1 + c_p / c_n\right)^{-1}$, and using the formula (5) one can conclude that this can take place for very high DC excitation level with $n_o \approx p_o$ and $n_o, p_o >> n_1, p_1$. Fig. 2 shows f_0 and Y_0 for both $\Lambda = 0$ and $\Lambda \neq 0$. A discrepancy between both cases becomes apparent for levels located at midgap and upper part of the bandgap. Therefore, in this approach, electron τ_n and hole τ_p lifetimes are assumed to be different, hence four parameters characterize the recombination process, i.e. concentration N_r, activation energy E_r, and electron, hole capture cross sections σ_n, σ_p. Two additional parameters, diffusivity D_n and surface recombination velocity v_s describe the carrier transport in the material. The investigation of the relation between the microwave spectra and the above parameters begin with expressing the occupancy function f_r in more convenient form:

$$f_r = \frac{n_o + \eta p_1}{n_o + n_1 + \eta(p_o + p_1)} \tag{16}$$

where $\eta = \sigma_p/\sigma_n$. It is seen that f_r depends on two parameters, E_r and η, instead of E_r, c_n and c_p. Introducing a new variable $\chi = c_n N_r$ the electron/hole lifetimes can be expressed as follows:

$$\tau_n^{-1} = \chi(1 - f_r), \qquad \tau_p^{-1} = \eta\chi f_r \tag{17}$$

where relations (4) are used. Now free carrier kinetics is characterized by three parameters E_r, η, and χ. However, microwave reflection coefficient further depends on N_r via delay parameter M, which now has the form:

$$M = \chi\left[n_o + n_1 + \eta(p_o + p_1)\right] / N_r \tag{18}$$

thus $\widetilde{R}(\omega)$ still depends on six parameters E_r, η, χ, N_r, v_s, and D_n; but now we expect that some of them are less influential. To explore the dependence between the each parameter and $\widetilde{R}(\omega)$, the f_0 and half width at half maximum (HWHM) functions are investigated. These functions are calculated at 25^0C and 240^0C and they are drawn in Figure 3. In Fig. 3a the function f_0 vs. E_r is plotted again, in order to illustrate how E_r affects the microwave spectra in comparison to other parameters, f_0, HWHM variations are larger at lower temperature than at elevated for shallow levels. Fig. 3b shows f_0, HWHM vs. η, and η affects the spectra only at elevated temperatures. The dependence between f_0 and χ in log-log scale is linear and the slope is temperature independent as shown in Fig.3c. Surface recombination velocity above the value of ~100cm/s

affects f_0 and HWHM, as shown in Fig. 3d. Therefore, this parameter cannot be properly evaluated for v_s smaller than 100cm/s. The last two Figures, e and f, demonstrate that f_0 and HWHM do not depend on D_n and N_r (below 10^{13} cm^{-3}) at both temperatures; they are thus kept constant at 10 cm^2/s and 10^{11} cm^{-3}, respectively. Henceforth, four variables v_s, χ, η, and E_r are used for spectra simulation. Among them, two are material parameters viz. η, E_r, while v_s, χ depend on the surface quality and recombination center concentration. Two valuable conclusions in the evaluation of the deep levels can be drawn from the analysis of Fig. 3: (i) midgap levels measurement should be carried out at elevated temperatures; in this case two materials parameters can be evaluated E_r and η, and (ii) shallow levels should be measured at room temperatures, with the evaluation of E_r only.

In the curve fitting procedure, a common difficulty is the numerical minimization of the error function $\chi(\vec{a})$ due to the presence of local minima. Often the final solution depends on the value of initial guess $\vec{a}_0$, where $\vec{a}$ is a multi-dimensional fitting vector. Since the multi-dimensional fitting procedure sometimes creates false output results, it is convenient to investigate the solution as a function of well-controlled physical parameters of the system, such as temperature or DC excitation levels in order to gain a more accurate assessment. In this work, the temperature has been chosen as a control parameter and the normalized quadrature component $Y(\omega)/Y_0$ is used for parameter evaluation. The accuracy of the fitting procedure was tested by simulation of the spectra with added random component: $\mathbf{R}_{\mathrm{ac}}(\omega) = R_{ac}(\omega)(1 + C\mathbf{r})$, where C describes a tool error. This error was assumed to be 1% of the measured signal, while $\boldsymbol{r}$ is uniformly distributed random number within (0, 1) range. A fitting procedure has been carried out using a minimization of the objective function:

$$\chi^2(\vec{a}) = \sum_T \sum_f \left(\frac{Y(f,T)}{Y_o} - \frac{Y_{EX}(f,T)}{Y_{oEX}} \right)^2 \tag{19}$$

with application of nonlinear simplex method. The components $Y(\omega)$ and $Y_{EX}(\omega)$ are the normalized model and measured quadrature voltage, respectively. In order to study the solution robustness, the fitting process was carried out with different initial guess vector $\vec{a}_0$. It has been confirmed that the procedure with fitting vector of [v_s, χ, η, E_r] leads to the stable solution, while the [v_s, σ_n, σ_p, E_r, N_r] results are not unique.

MEASUREMENT AND SEMICONDUCTOR EVALUATION

The procedure described in Section II, was used to evaluate the parameters for contaminated p-type Si wafers having a boron doping concentration of about 10^{15} cm^{-3}. The wafer sets were intentionally contaminated with Fe and Ni to a concentration of ~ 10^{11} and 10^{12} cm^{-3}, respectively. The measurement system set-up was described in our previous papers[14,16]. Figure 4 shows the measured quadrature spectra for wafers containing iron with concentrations of 5x10^{11} cm^{-3} and 5x10^{12} cm^{-3}, respectively. For low contamination the maximum value of Y_o increases from RT to 100°C, decreases in the range 100°C to 180°C, and increasing again for temperature exceeding 180°C. A decrease in the value of Y_o in the temperature range100°C to 180°C, indicates the presence of active shallow level activity according to Fig. 2b, while an increase in

Y_o, above 180°C, indicates the presence of effective deep levels. For samples having a high iron concentration of $5x10^{12}$ cm^{-3}, the low frequency spectra increase between 20°C and 60°C due to presence of Fe-B levels, which become inactive at temperatures in excess of 100°C. The value of Y_o raises at high frequency range at temperatures between 20°C to 60°C, indicating an active deep level. The decrease of Y_o between 60°C and 180°C is due to effective shallow level or the electron capture cross section variation. Above 180°C the effect of the deep level becomes dominant.

In order to determine the activation energy E_r, and parameters η and χ, the procedure described in section II was used with spectra measured for two different temperatures. The robust parameters, which were evaluated for temperatures above 180°C and 240°C, are listed in Table I. The activation energy of the Fe contaminated wafers #2 and #3 is equal to 0.5eV, while the electron/hole capture ratio is about 0.03. It is instructive to note that in this case, the ratio of high to low Fe contents $\chi(\#3)/\chi(\#2) \approx N_r(\#3)/N_r(\#2) = 7.2$ follows approximately the ratio $N_r(\#3)/N_r(\#2) = 13.3$ of iron-boron pair concentration measured using DLTS. In the case of Fe(50%) + Ni(50%) contamination of the sample #7, both E_r and η are similar to the values for samples contaminated with Fe, indicating that recombination process is controlled by iron centers. The activation energy of 0.5eV was also evaluated for the REF sample #1, but with different value of $\eta = 0.046$, suggesting a different recombination mechanism than for Fe samples #2 and #3. Different values of the activation energy $E_r = 0.53$eV and capture cross section ratio $\eta \approx 0.048$ were found for the wafer containing Ni, wafer #5.

Table I shows two additional parameters N_r and τ measured using DLTS and μ-PCD, at temperatures about 50K and 300K, respectively. The DLTS spectra shown in Figure 5 were measured using Al Schottky barrier of 1 mm in size and temperature range from 40K to 290K. Fe-B deep levels are seen for Fe contaminated wafers #2 and #3 and for Fe+Ni contaminated wafer #7. The DLTS spectra for the REF wafer #1 and the Ni contaminated wafer #5 do not provide evidence of the presence of deep levels. The Fe-B concentration ratio $N_r(\#3)/N_r(\#7) = 1.3$ for Fe and Fe+Ni wafers is almost equal to ratio $\chi(\#3)/\chi(\#7) = N_r(\#3)/N_r(\#7) = 1.6$, evaluated using FR-PC. With the exception of the REF wafer, the value of χ^{-1} evaluated using FR-PC is the same order as the lifetime τ, measured using μ-PCD method. The discrepancy between χ^{-1} and τ for the REF wafer is due to high DC injection level. Indeed, from Eqs. (16) and (17):

$$\tau_n = \left(1 + \frac{n_o + \eta p_1}{n_1 + \eta p_o}\right)\chi^{-1}$$

thus $\tau_n = \chi^{-1}$ for low DC injection level and midgap recombination centers. On the other hand, for the high DC injection level and small η, $\tau_n = (\eta\chi)^{-1}$ demonstrating that τ_n can differ essentially from χ^{-1}. The surface recombination velocity v_s, not shown in the tables, was determined to be less than 100 cm/s for all analyzed cases.

SUMMARY AND CONCLUSION

The microwave photoconductance method has been investigated in the context of wafer characterization. The relation for microwave reflection coefficient in the frequency domain is found. Single level Shockley-Read-Hall non-stationary recombination model is used for the description of the carrier kinetics. Six parameters, which characterize the process such as, surface recombination velocity v_s, diffusivity D_n, activation energy E_r, electron/hole capture cross sections σ_n, σ_p, and concentration N_r are analyzed. It is shown that only four are robust; namely v_s, E_r, $N_r c_n$ and σ_p/σ_n, and among them two, E_r and σ_p/σ_n, can be used as material parameters. These two parameters are evaluated from the frequency resolved spectra for silicon wafers intentionally contaminated with Ni and Fe. The E_r and σ_p/σ_n values obtained for Fe, and Fe+Ni contaminated wafers were equivalent, while in the presence of Ni, the above parameters were different, indicating that these parameters can be used for material characterization. The variation of the concentration evaluated from the third parameter χ follows the Fe-B pair variation measured using DLTS, proving the validity of the described method. It was found that the activation energy at a temperature of about 200^{o}C for Fe contaminated p-type CZ Si wafers is equal 0.5eV. A similar value was predicted by Istratov[22] et al, using quadrature approximation of the experimental data evaluated at low and high temperatures.

REFERENCES

[1]Y. Kirino, A. Buczkowski, Z.J. Radzimski, G.A. Rozgonyi, and F. Shimura, Appl. Phys. Lett. **57**, 2832 (1990).

[2]C.H. Ling, and Z.Y. Cheng, Appl.Phys. Lett. **71**, 3218 (1997).

[3]C. Kaniava, E. Gaubas, J. Vaitkus, J. Vanhellemont, and A.L.Rotondaro, Matr. Science and Technology **11**, 670 (1995).

[4]T.S. Horanyi, P. Tutto, and Cs. Kovacsics, J. Electrochem. Soc. **143**, 216 (1996).

[5]Y. Marfaing, *Photoconductivity Photoelectric Effects*, **Handbook on Semiconductors,** Vol.2 (ed. M. Balkanski) North-Holland 1994.

[6]M. Ichimura, H. Tajiri, T. Ito, and E. Arai, J. Electrochem. Soc. **145**, 3265 (1998).

[7]E. Gaubas, A. Kaniava and J. Vaitkus, Semicond. Sci. Technol. **12**, 1 (1997).

[8]K. Graff, *Metal Impurities in Silicon-Device Fabrication*, Springer-Verlag, Berlin 1995.

[9]S.A. McHugo, R.J. McDonald, A.R. Smith, D.L. Hurley, E.R. Weber, Appl. Phys. Lett. **73**, 1424 (9998).

[10]D. Gilles, W. Schroter, W. Bergholz, Phys. Rev. B **41**, 5770 (1990).

[11]T. Otaredian, Solid-St. Electronics **36**, 153 (1993).

[12]T. Otaredian, *Contactless Microwave Lifetime Measurement*, Thesis, Technische Universiteit Delft, 1992.

[13]R. Schieck, and M. Kunst, Solid-St. Electron. **41**, 1755 (1997).

[14]A. Romanowski, A. Buczkowski, N. Sukidi, and G. Rozgonyi, *Measurement of Trapping Centers in Crystalline Si by Frequency Resolved Laser Microwave Photo Conductance Decay*, AIP Conf. Proc. 353, 13-th NREL Photovolt. Program Review, Lakewood, CO 1995, pp. 545.

[15]A. Romanowski, A. Buczkowski, A. Karoui and G. Rozgonyi, in *Silicon Recombination Lifetime Characterization Methods*, ASTM STP 1340, F.Bacher and W.H.Hughes Eds. (1998), pp. 68.
[16]A. Romanowski, A. Buczkowski, A. Karoui, and G. Rozgonyi, J. Appl. Phys., **83**, 7730 (1998).
[17]W.H. Press, S.A. Teukolsky, W.T. Vetterling, and B.P. Flannery, *Numerical Recipes in Fortran*, Cambridge, 1994.
[18]S.M. Sze, *Physics of Semiconductor Devices*, Wiley Interscience, New York 1969.
[19] Orton and P. Blood, *The Electrical Characterization of Semiconductors: Measurement of Minority Carrier Properties*, Academic Press, 1990.
[20]D. K. Schroder, *Semiconductor Material and Device Characterization*, Wiley & Sons Inc., 1998.
[21]M. A. Lourenco and K. P. Homewood, Semicond. Sci. Technol. **8**, 1277(1993).
[22]A.A. Istratov, H. Hieslmair, and E.R. Weber, *9-th Workshop on Crystalline Silicon Solar Cell Materials and Processes*, p. 16, Beaver Run Resort, Breckenridge, Colorado 1999.

APPENDIX

The diffusion equation (10a) for free electrons with band-to-deep level transient component (2b) can be written in the time domain as:

$$\frac{\partial n}{\partial t} = g_n + D_n \frac{\partial^2 n}{\partial x^2} - c_n n(N_r - n_r) + c_n n_r n_1 \tag{A.1}$$

which in the frequency domain and with linear approximation has the form:

$$i\omega\tilde{n} = \tilde{g} + D_n \frac{\partial^2 \tilde{n}}{\partial x^2} - \frac{\tilde{n}}{\tau_n} + \beta\tilde{n}_r \tag{A.2}$$

Inserting Eq. (9) to Eq. (A.2) one can obtain the diffusion equation (10b).

Table I. Recombination Center Properties

Wafer	Determined by FR-PC @ 180 °C and 240 °C				**DLTS** @ 50 K	**PCD** @ 21°C
	E_r	η (σ_p/σ_n)	χ $(N_r\, c_n)$	χ^{-1}	N_r	τ
	[eV]	[1]	[s^{-1}]	[μs]	[cm^{-3}]	[μs]
#1 (REF)	0.50	0.046	$7.9\text{x}10^3$	126.6		70
#2 (Fe)	0.50	0.030	$1.3\text{x}10^5$	7.7	$3\text{x}10^{11}$	5.5
#3 (Fe)	0.50	0.026	$9.4\text{x}10^5$	1.06	$4\text{x}10^{12}$	1.5

#5 (Ni)	0.53	0.048	4.5×10^4	22.2		20
#7 (Fe + Ni)	0.50	0.029	6.0×10^5	1.7	3×10^{12}	2.2

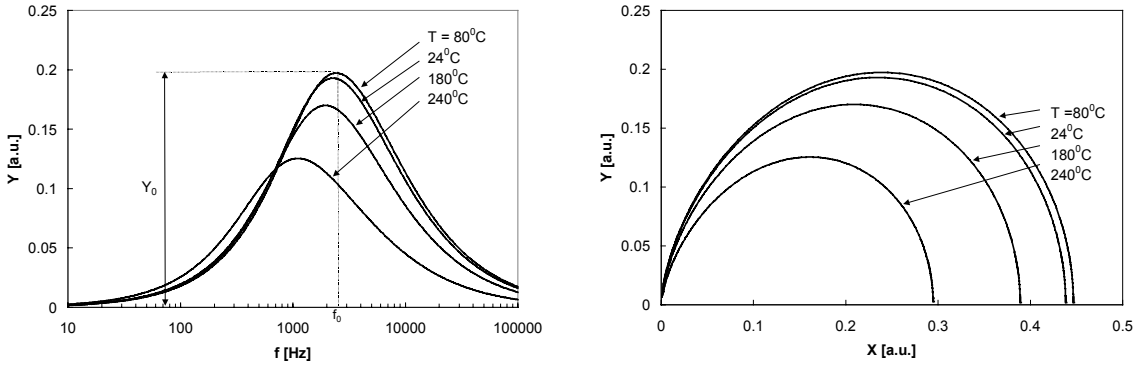

(a) (b)

Fig. 1. (a) Quadrature spectra $Y(\omega)$, and Nyquist plots (b) simulated using Eq. 15. Plots are given as a function of temperature (24, 80, 180 and 240° C), for $v_s = 10^3$ cm/s, $\sigma_n = \sigma_p = 10^{-15}$ cm^2, $N_r = 10^{12}$ cm^{-3}, and $E_r = 0.4$eV.

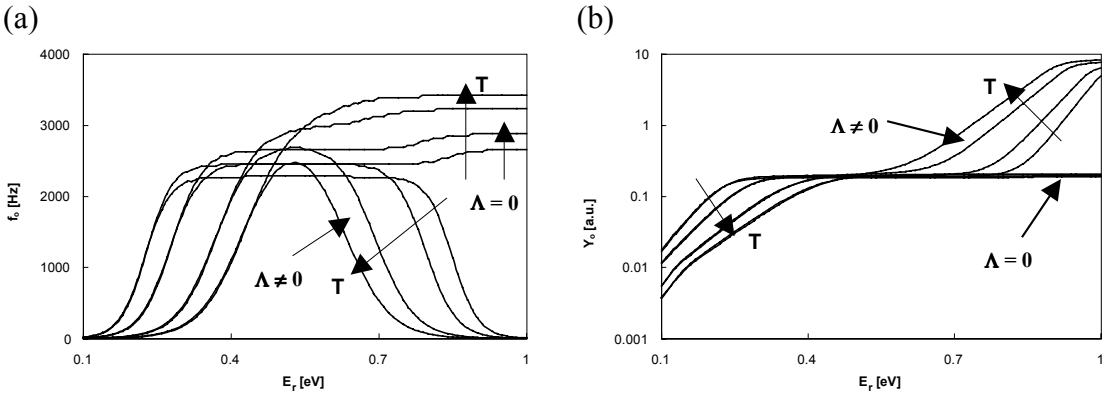

Fig. 2. Simulated dependence of (a) f_0 and (b) Y_0 versus activation energy E_r at temperature 24 ^{0}C, 80 ^{0}C, 180 ^{0}C and 240^{0}C, with $\Lambda = 0$ and $\Lambda \neq 0$ ($v_s = 10^3$ cm/s, $\sigma_n = \sigma_p = 10^{-15}$ cm^2, $N_r = 10^{12}$ cm^{-3}, $E_r = 0.4$eV).

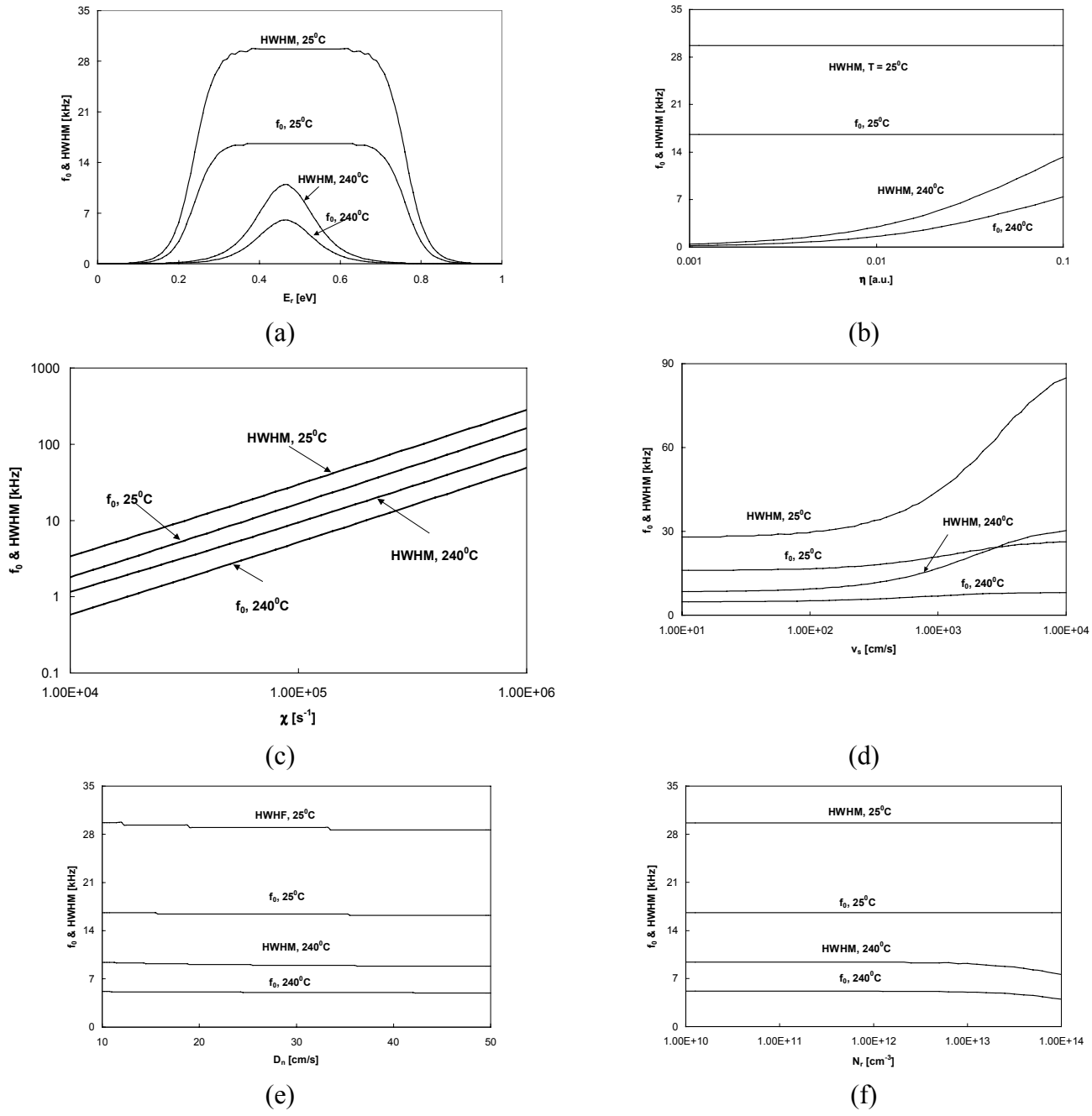

Fig. 3. Simulated f_0 and half width at half-maximum (HWHM) versus (a) activation energy E_r, (b) $\eta = \sigma_p/\sigma_n$, (c) $\chi = c_n N_r$, (d) surface recombination velocity v_s, (e) diffusivity D_n, and (f) concentration N_r; at temperatures 25 ^{0}C and 240^{0}C.

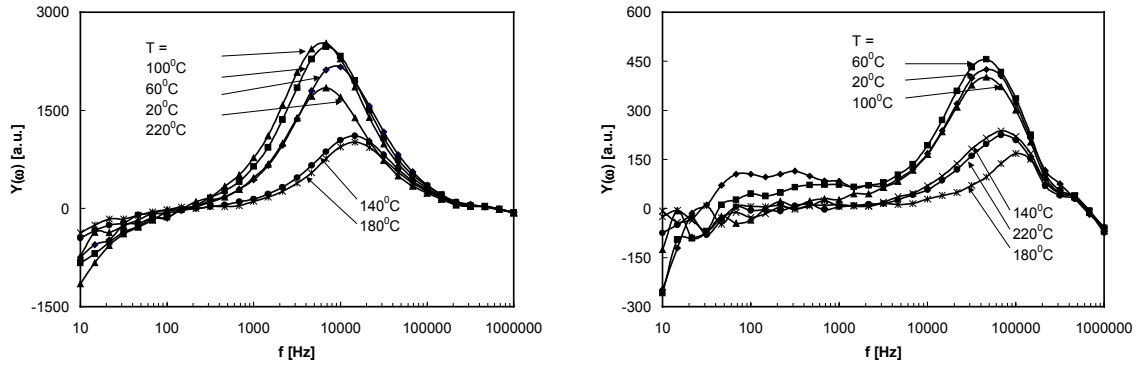

(a) (b)

Fig. 4. Measured quadrature spectra measured at 20^0, 60^0, 100^0, 140^0, 180^0, 220^0C for p-type silicon containing **Fe** impurities, (a) wafer #2, (b) wafer #3.

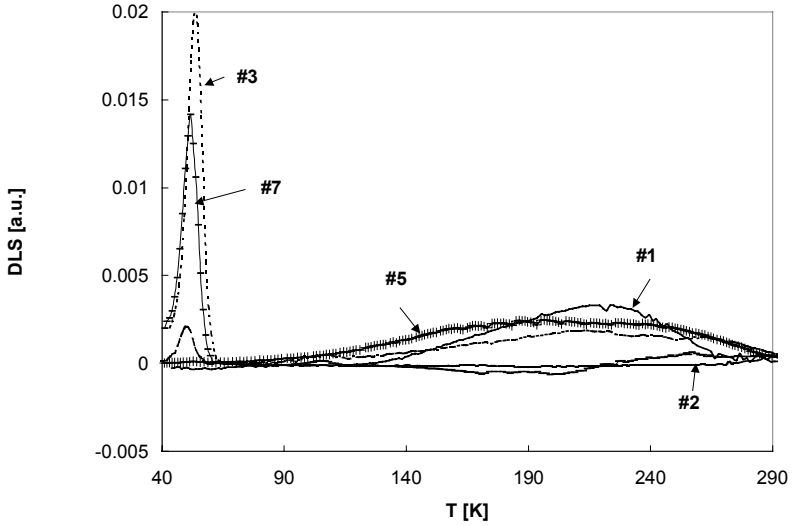

Fig. 5. DLTS spectra of reference wafer #1, Fe contaminated wafers #2, #3, Ni contaminated wafer #5, and Ni + Fe contaminated wafer #7.

Chapter 3

Gettering and Surface Reflectivity of Ti Thin Films

INTRODUCTION

Previously, we reported [1,2,3] that the best improvement of carrier lifetime was for TiN_xO_y film getter; therefore, this film was again evaporated for 45 min. In addition, Ti and TiN_x films were also evaporated and investigated. In this paper, we report on the optical properties of the Ti, TiN_xO_y and TiN_x nitride gettering ability and structural behavior of the film following a annealing process. The long-term temperature treatment used for external gettering can modify the optical properties of the film because of surface reconstruction, new phase formation, and evaporation; therefore, it is important to investigate the film properties before and after thermal treatment.

EXPERIMENTS

The films were prepared at room temperature by pulsed magnetron sputtering onto (100) Si substrate contaminated with iron. The Ti films were deposited in a 2mTorr Ar plasma containing diluted gasses of 1mTorr each of oxygen and nitrogen gases. The initial vacuum was $5x10^{-6}$ Torr and the Ti target was pre-cleaned in Ar plasma for 3min. The films were deposited for 45 min using a target current of 0.3A. The gettering-annealing process was performed in the same gas ambient as for Set #2, at 700^0C for 150min, with the nitrogen and oxygen gas flows of 7200sccm and 720sccm, respectively.

RESULTS

After gettering-annealing processes the films were examined by AFM and optical reflectometer. Then the films were stripped off using CP-4 solution for further investigations, which included the μ-PCD lifetime and the DLTS measurements. The film surface measurements were carried out using an AFM D-3000 in tapping-contact mode with a silicon cantilever probe in ambient air covering 1 x 1 or 5 x 5 μm^2 scanning areas. For each case the rms-roughness was evaluated. The rms data are presented in Table I and 2D AFM images are shown in Fig.1. The minimum roughness of 1.97nm is obtained for the TiN_xO_y film, while a maximum roughness of 10.70nm for the Ti film is obtained. 3D AFM images of the films (see Fig.2) show that the Ti film surface roughness is larger than for TiN_x and TiN_xO_y. Note that introducing N_2 and O_2 gases to the plasma diminishes the surface roughness. The grain size is larger than before annealing. Note that unique "worm-like" patterns are formed for the TiN_xO_y sample, while these patterns are not seen for the Ti and TiN_x films. The driving force for pattern formation lies in the adatoms diffusion during deposition and thermal annealing. Indeed, strong bonding between Si and Ti atoms is reduced after adding oxygen gas into the plasma due to high oxygen reactivity towards Ti atoms. As a result, film adhesion to substrate is much weaker than

in the case of Ti or TiN_x films. Secondly, segregation of the atoms at edge [4] of the grains diminishes surface energy and resulting in grain enhancement during the gettering annealing process. In the case of Ti film, the strong bonding between substrate silicon atoms and Ti atoms does not allow for surface adatoms diffusion processes, therefore small columnar grains are formed during deposition and growth [5]. On the other hand, the nitrogen atoms added to Ar plasma segregate at crystalline grains and they increase surface energy, resulting in lowering of grain growth compared to growth of Ti grains. It should be mentioned that a weak TiN_xO_y film adhesion to substrate is also seen during the film stripping process . After CP-4 etching, the surface becomes smooth for TiN_xO_y films only, and is rough after stripping Ti or TiN_x films.

The model F20-UV thin film optical system manufactured by Filmetrics, Inc. has been used for measuring wafer reflectance. The reflectance spectra were measured in the wavelength region from 224 to 845 nm.

Table I, Roughness Analysis

Film	Ti	TiN_x	TiN_xO_y
RMS [nm]	10.70	5.48	1.97

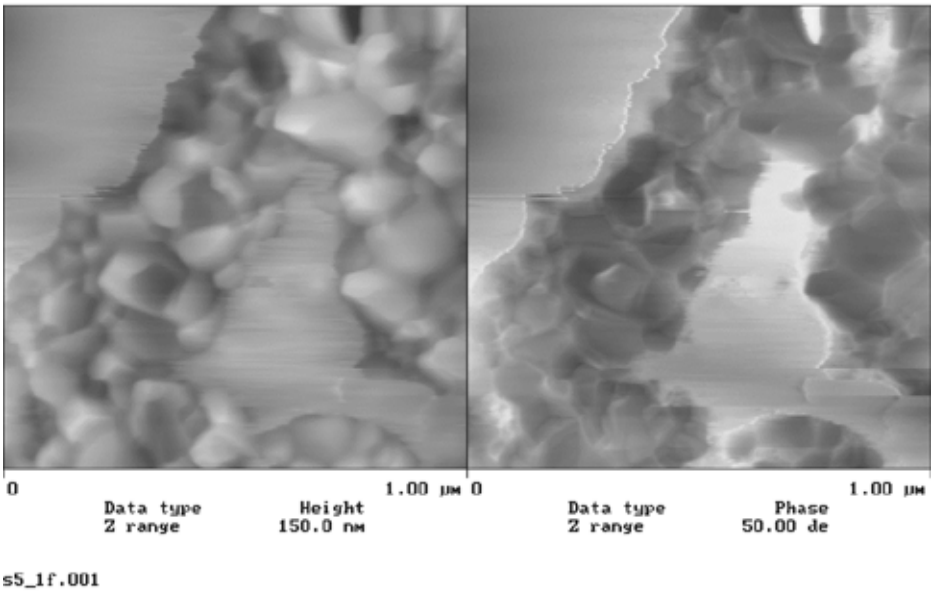

(a)

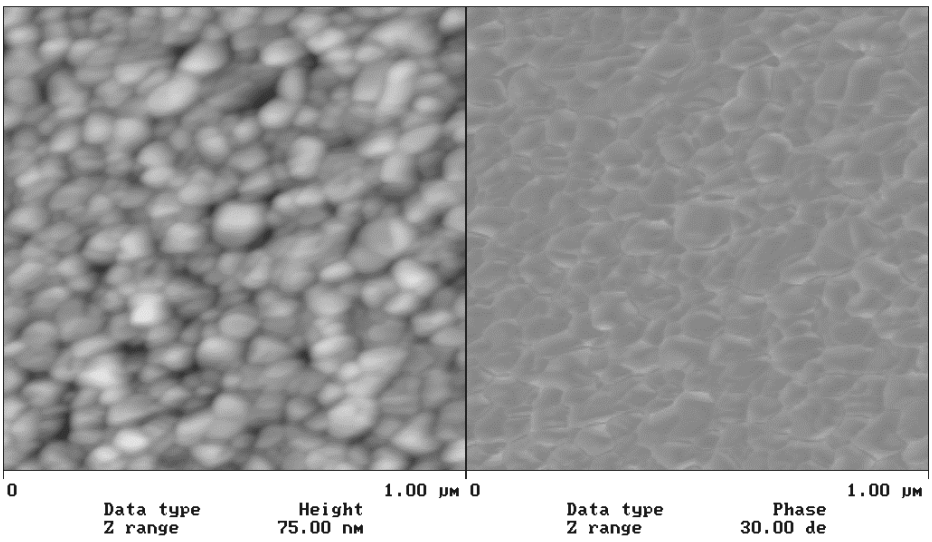

(b)

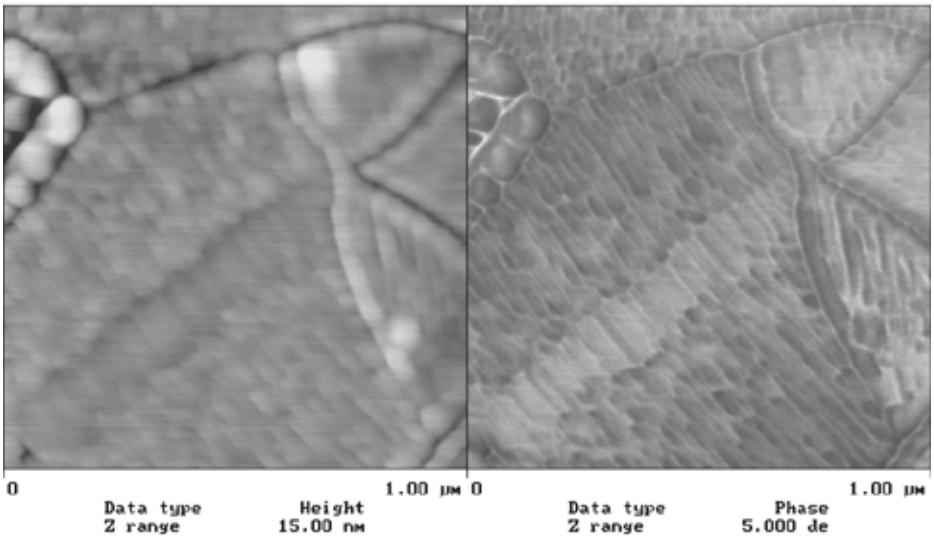

(c)

Fig. 1. 2D AFM images of annealed Ti films, (a) Ti/Ar; (b) TiN_x/Ar & N_3, (c) TiN_xO_y/Ar & N_2, O_2,

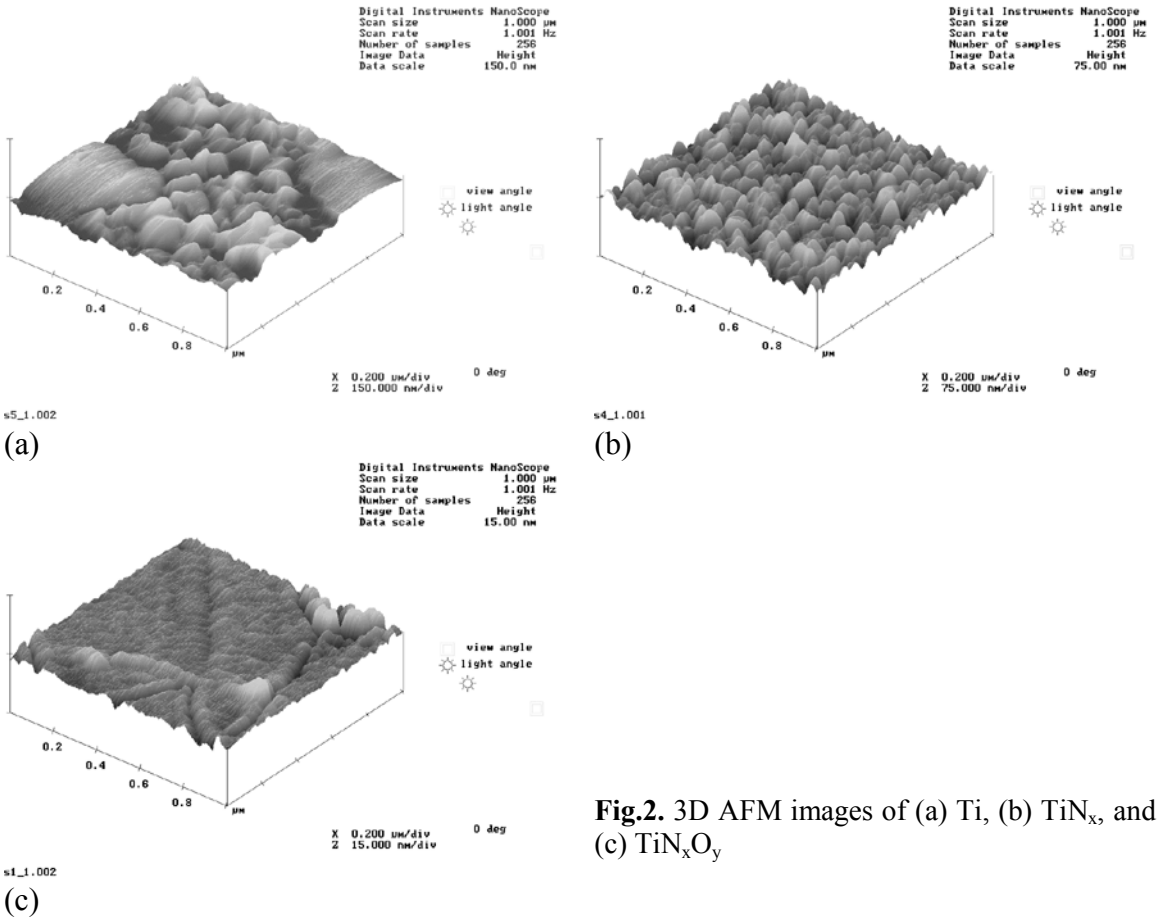

Fig.2. 3D AFM images of (a) Ti, (b) TiN_x, and (c) TiN_xO_y

The reflectance spectra of the non-annealed samples are presented in Fig. 3a. A long-wavelength reflectivity of 0.1 is seen for the TiN_xO_y film. In the case of Ti and TiN_x films, the reflectance increases with increasing wavelength, and reaches a value of about 0.4 for Ti film due to the presence of metal atoms. After annealing, most of the spectra changed, as shown in Fig. 3b. Only the TiN_xO_y film spectrum remained the same indicating good thermal stability of the film. In the modeling of the reflectance spectra, the Drude-Lorentz (D-L) oscillator [6] and Forouhi-Bloomer (FB) [7,8] models were implemented. In both cases the dielectric function (DF) was simulated by a combination of the single-layer on an absorbing substrate using Fresnel's equations [9] and DL or FB equations. In the Forouhi-Bloomer approaches, the refractive index n and the extinction coefficient k have the following forms:

$$n(E) = n_\infty + \frac{B_o E + C_o}{E^2 - BE + C}, \quad k(E) = \frac{A(E - E_o)^2}{E^2 - BE + C} \tag{1}$$

$$B_o = \frac{A}{Q}\left[-\frac{B^2}{2} + E_o B - E_o^2 + C\right], \; C_o = \frac{A}{Q}\left[(E_o^2 + C)\frac{B}{2} - 2E_o C\right], \; Q = \frac{1}{2}(4C - B^2)^{1/2}$$

The FB simulated and experimental spectra are shown in Fig. 4. The model matches well in the long wavelength range with the experimental data for Ti and TiN_xO_y films, as shown in Fig. 4a and c.

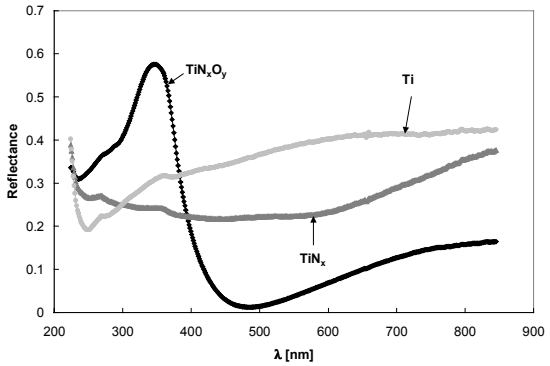

(a)

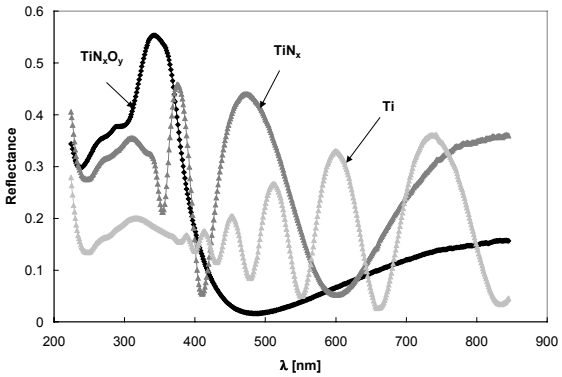

(b)

Fig. 3. The reflectance of non-annealed (a) and annealed (b) wafers.

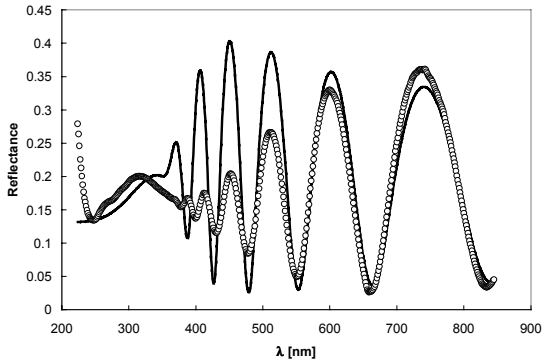

(a)

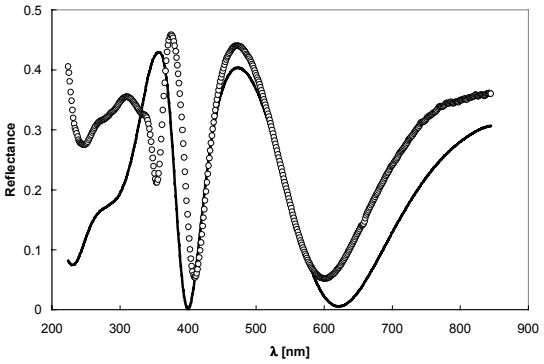

(b)

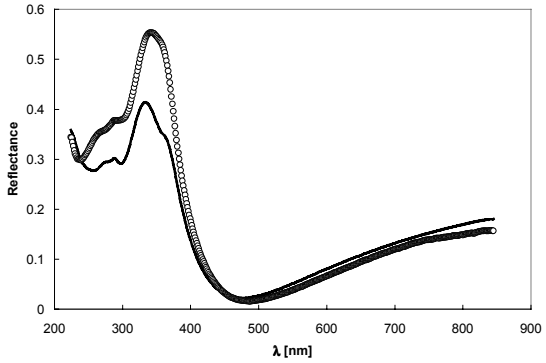

(c)

Fig. 4. Experimental (open dots) and calculated (solid lines) spectra using FB method, (a) Ti, (b) TiN_x, and (c) TiN_xO_y.

Table II Parameters obtained from a FB fit

Sample	A	B [eV]	C [eV^2]	E_0 [eV]	n_∞	d [nm]	Error [%]
Ti	0.05	7.62	15.02	1.58	2.18	628.5	0.6469
TiN_x	0.06	7.56	14.68	2.18	2.00	219.0	0.9072
TiN_xO_y	0.10	7.58	14.56	2.81	2.26	50.0	0.3870

The error function shown in the last column of the table is defined as follows:

$$Error[\%] = \frac{100}{N}\sqrt{\sum_{j=1}^{N}\left(\frac{R_j^{TH} - R_j^{EX}}{R_j^{EX}}\right)^2} \tag{2}$$

where R_j^{TH} and R_j^{EX} are simulated and measured reflectance, respectively. The evaluated optical bandgap, see Table II, of 2.81eV for TiN_xO_y film agrees well with literature data [10] for crystalline TiO_x film, which varies from 1.44 eV to 2.73 eV depending on film thickness, and from 2.88 to 3.07 eV for amorphous film. Second parameter for TiN_xO_y, $n_\infty = 2.26$, differs from literature data $n_\infty = 2.05$ [10]. In the case of Ti and TiN_x films, both FB or DL models have been used for the simulation of the reflectance spectra. In the DL approach [6] the plasma and one resonance frequencies have been used for modeling the dielectric function:

$$\varepsilon = \varepsilon_\infty + \frac{\Omega^2}{\Omega_o^2 - \omega^2 - i\omega\gamma} - \frac{\omega_p^2}{\omega^2 + i\omega\tau^{-1}} \tag{3}$$

The reflectance spectra simulated using DL and FB models for Ti and TiN_x films are shown in Fig 5, and the error function calculated using Eq. (2) is higher for DL than for the FB model. Plasma energy and relaxation time for those films are similar and equal 4.4eV and $10^{-13.9}$ sec, respectively. The calculated plasma energy is two times larger than that for TiN film (2.6eV) [5], τ is typical for conductive materials [6]. We expect that stronger bonds between Ti and O atoms compared to Ti-N bonds resulted in the reduction of the plasma frequency; therefore, formation

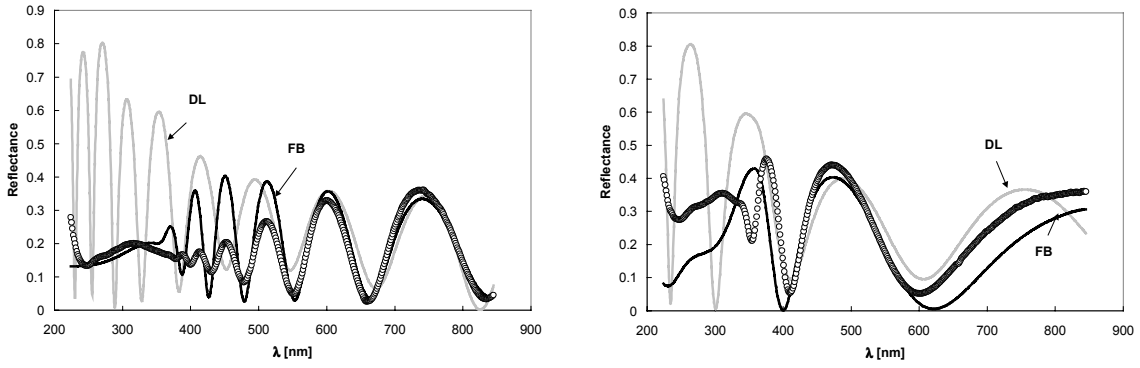

(a) (b)

Fig. 5. Experimental (open dots) and calculated (solid lines) DL and FB spectra (a) Ti, (b) TiN_x

of the TiO_x film should lead to plasma energy reduction rather than increasing. Thus the DL model does not match the measured spectra and the FB model must be used. In this case, the optical bandgap, see Table II, were determined to be 1.58eV, 2.18eV for Ti and TiN_x films, respectively.

LIFETIME EVALUATION

The effectiveness of the gettering procedure has been examined by measuring the carrier lifetime. The carrier lifetime was measured using μ-PCD JANUS 300 under low (in Automatic Mode) excitation level. Before measurement, the films were stripped using CP-4 solution and then dipped in HF solution in order to passivate broken bonds. The reference sample lifetime was 70 μsec and after iron contamination, the lifetime decreased to 9.0 μsec. The lifetime data for the gettered samples are present in Table III. The bulk lifetime increased from 9 μsec to 14.5 μsec for Ti and TiN_x films, and decreased for the TiN_xO_y film as shown in Table III.

Table III Lifetime measurements

Sample	τ [μsec]	$\frac{\Delta\tau}{\tau}$ [%]
TiN_xO_y	8.5	
TiN_x	14.5	37.9
Ti	14.5	37.9

Because of the stronger bonding of Ti to O atoms than to Si atoms from the substrate, the interface between substrate and film is not efficient enough for external gettering.

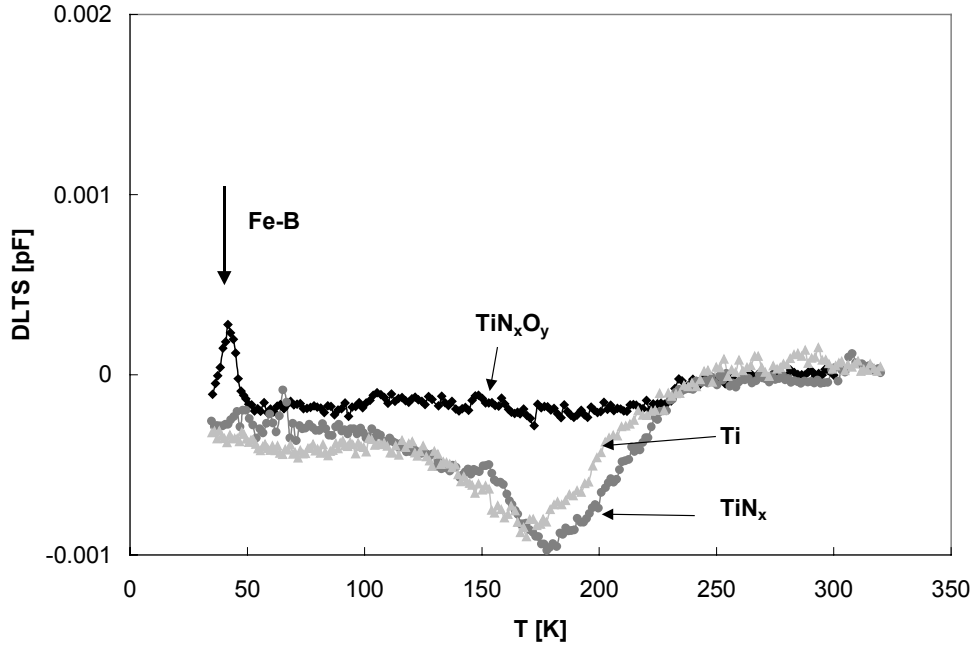

Fig. 6. Measured DLTS spectra of Fe contaminated Si wafers with Ti, TiN_x and TiN_xO_y films

Prior to Schottky barrier deposition, the samples were cleaned in piranha etching for 2 min and dipped in HF solution. Next Ti diodes of 1 mm diameter were evaporated followed by Al evaporation to a thickness of 1500A. The diode qualities were examined by measuring the C-V and I-V characteristics. DLTS spectra are shown in Fig. 6.. The Fe-B peak of $N_{Fe-B} = 8.7x10^{10}$ cm^{-3} is only seen for wafer covered with TiN_xO_y film. Broad negative signal visible on the picture is generated by film-silicon interface and was not detected for both non-gettered and gettered with TiN_xO_y film samples. The Fe-B peak, not shown in the figure, of $5x10^{12}$ cm^{-3} has been detected for non-gettered sample.

DISCUSSION AND CONCLUSIONS

Optical and gettering properties of the three films Ti, TiN_x and TiN_xO_y have been investigated. The TiN_xO_y film reveals the best optical quality; however, poor interface formation between the film and surface due to strong Ti and O bonds eliminates that film as a good external getter. Poor gettering properties of the film are indicated by lifetime deterioration and iron concentration about 10^{11} cm^{-3}. Both Ti and TiN_x films have good gettering properties, however they reveal poor optical parameters. The long wavelength reflectance for both films is high and reaches the value between 40 to 50%. Short wavelength reflectance of 20% for Ti film is lower than the reflectance for TiN_x film and is probably caused by surface roughness which is the largest for Ti film. After gettering thermal treatment semiconducting films are formed with optical bandgap between 1.6eV and 2.8eV.

REFERENCES

1. A. Romanowski, J. Kasichainula, J. Muth, and G. Rozgonyi, *NCPV Program Review Meeting 2000*, Denver 2000, p.151.
2. A. Romanowski and G. Rozgonyi, *9th Workshop on Crystalline Silicon Solar Cell*, Breckenridge 1999, p.218.
3. A. Romanowski, J. Kasichainula, and G. Rozgonyi, 10th *Workshop on Crystalline Silicon Solar Cell Materials and Processes*, Colorado 2000, p. 224.
4. D.L. Smith, *Thin-Film Deposition,* McGraw-Hill, New York 1995.
5. S. Logothetidis, et al, Thin Solid Films **338**, 304(1999).
6. G.R. Fowles, *Introduction to Modern Optics*, Dover Publ., Inc., New York 1975.
7. A.R. Forouhi and I. Bloomer, Physical Rev. B **34**, 7018(1986).
8. A.R. Forouhi and I. Bloomer, Physical Rev. B **38**, 1865(1988).
9. O.S. Heavens, *Optical Properties of Thin Solid Films*, Dover., New York 1991.
10. J. Rodriguez, M. Gomez, J. Ederth, G.A. Niklasson, and C.G. Granqvist, Thin Solid Films **365**, 119(2000).

REPORT DOCUMENTATION PAGE

Form Approved
OMB NO. 0704-0188

1. AGENCY USE ONLY (Leave blank)	2. REPORT DATE	3. REPORT TYPE AND DATES COVERED
	June 2002	Final Subcontract Report, 28 January 1998 – 28 August 2001

4. TITLE AND SUBTITLE
Characterization of and Ti Gettering for PV Substrates,
Final Subcontract Report, 28 January 1998 – 28 August 2001

5. FUNDING NUMBERS
CF: XAF-8-17607-03
PVP22501

6. AUTHOR(S)
G.A. Rozgonyi, A. Karoui, A. Romanowski, and L. Kordas

7. PERFORMING ORGANIZATION NAME(S) AND ADDRESS(ES)
North Carolina State University
Raleigh, North Carolina 27695-7916

8. PERFORMING ORGANIZATION REPORT NUMBER

9. SPONSORING/MONITORING AGENCY NAME(S) AND ADDRESS(ES)
National Renewable Energy Laboratory
1617 Cole Blvd.
Golden, CO 80401-3393

10. SPONSORING/MONITORING AGENCY REPORT NUMBER
NREL/SR-590-31983

11. SUPPLEMENTARY NOTES
NREL Technical Monitor: Robert McConnell

12a. DISTRIBUTION/AVAILABILITY STATEMENT
National Technical Information Service
U.S. Department of Commerce
5285 Port Royal Road
Springfield, VA 22161

12b. DISTRIBUTION CODE

13. ABSTRACT *(Maximum 200 words)*
This report describes two project objectives: to determine optical and gettering properties of titanium and titanium oxy-nitride films, and to examine the influence of carrier recombination processes on the microwave reflection coefficient in the frequency domain such that PV materials parameters could be evaluated nondestructively. A third topic was added as the main focus, wherein we carried out a detailed characterization study of dislocated, high-purity, float-zone crystals grown at NREL. These crystalswere compared with nitrogen-doped CZ wafers. The accompanying report has a chapter devoted to each of these topics: (1) characterization of controlled defect/impurity growth of float-zone crystals; (2) contactless characterization of silicon wafers using frequency-resolved photoconductance decay; and (3) gettering and surface reflectivity of Ti thin films.

14. SUBJECT TERMS: PV; Ti gettering; carrier recombination; float-zone crystals; microwave photoconductance; thin films; minority carrier; silicon wafers; Schottky barrier; optical bandgap; wavelength reflectance;

15. NUMBER OF PAGES

16. PRICE CODE

17. SECURITY CLASSIFICATION OF REPORT	18. SECURITY CLASSIFICATION OF THIS PAGE	19. SECURITY CLASSIFICATION OF ABSTRACT	20. LIMITATION OF ABSTRACT
Unclassified	Unclassified	Unclassified	UL